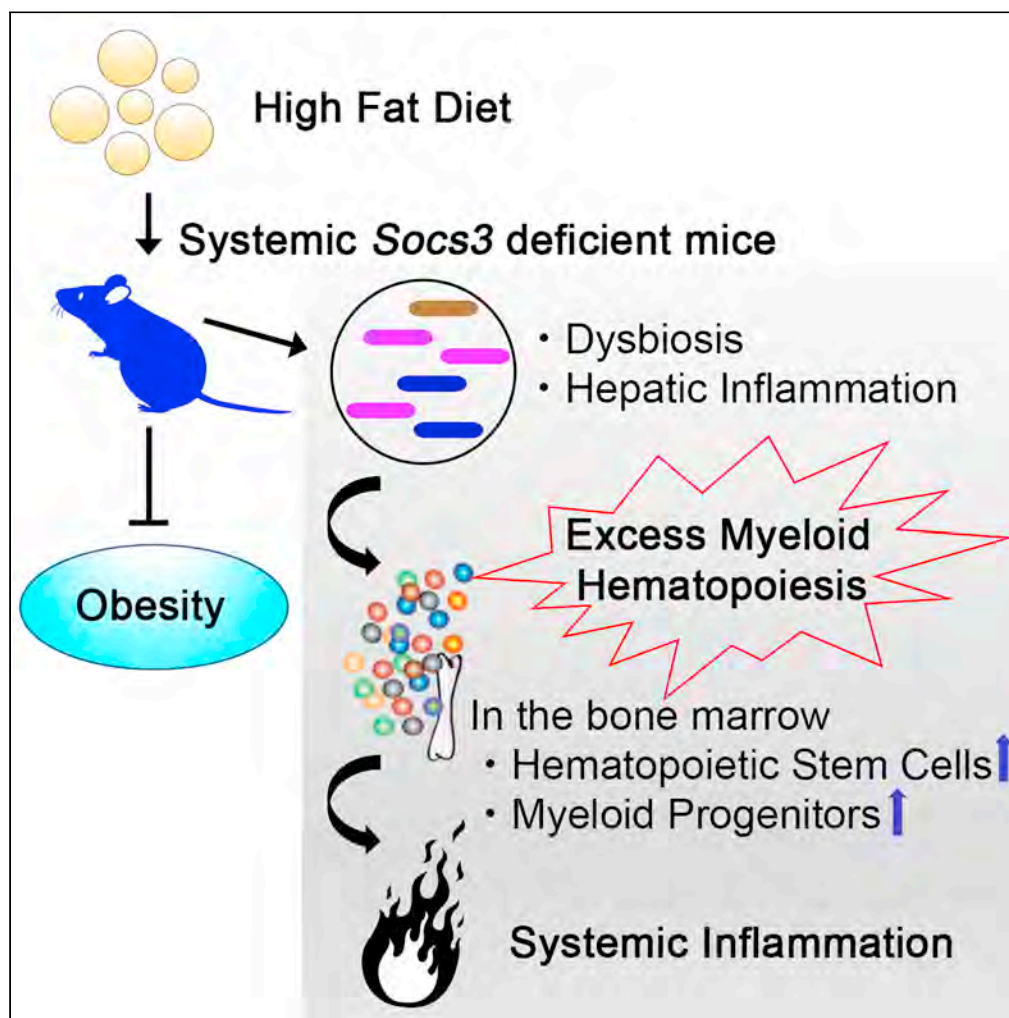**Article**

Altered microbiota by a high-fat diet accelerates lethal myeloid hematopoiesis associated with systemic SOCS3 deficiency

Kaori Cho, Takashi Ushiki, Hajime Ishiguro, ..., Warren S. Alexander, Hitoshi Shimano, Hirohito Sone

tushiki@med.niigata-u.ac.jp

Highlights

SOCS3 suppresses severe systemic inflammation associated with high-fat diet

SOCS3 deficiency on high-fat diet accelerates excess myeloid hematopoiesis

SOCS3 controls gut dysbiosis on high-fat diet

iScience

Article

Altered microbiota by a high-fat diet accelerates lethal myeloid hematopoiesis associated with systemic SOCS3 deficiency

Kaori Cho,[1,13] Takashi Ushiki,[1,2,14,*] Hajime Ishiguro,[1,13] Suguru Tamura,[1] Masaya Araki,[3] Tatsuya Suwabe,[1] Takayuki Katagiri,[1] Mari Watanabe,[2] Yoko Fujimoto,[2] Riuko Ohashi,[4,5] Yoichi Ajioka,[4,5] Ippei Shimizu,[6] Shujiro Okuda,[7] Masayoshi Masuko,[1] Yoshimi Nakagawa,[8] Hideyo Hirai,[9,10] Warren S. Alexander,[11,12] Hitoshi Shimano,[3] and Hirohito Sone[1]

SUMMARY

The suppressors of cytokine signaling (SOCS) proteins are negative regulators of cytokine signaling required to prevent excessive cellular responses. In particular, SOCS3 is involved in the regulation of metabolic syndromes, such as obesity and diabetes, by suppressing leptin and insulin signals. SOCS3 also suppresses the inflammatory response associated with metabolic stress, but this specific role remains undefined. Wild-type mice on a high-fat diet (HFD) exhibited only fatty liver, whereas systemic deletion of SOCS3 resulted in excessive myeloid hematopoiesis and hepatic inflammation. In addition, depletion of the gut microbiota resulted in considerable improvement in excess granulopoiesis and splenomegaly, halting the progression of systemic inflammation in SOCS3KO mice on the HFD. This result suggests that intestinal dysbiosis is involved in inflammation associated with SOCS3KO. Although contributing to diet-induced obesity and fatty liver, SOCS3 is nevertheless critical to suppress excess myeloid hematopoiesis and severe systemic inflammation associated with intestinal dysbiosis on HFD.

INTRODUCTION

High-fat diets (HFDs) accelerate chronic diseases such as type 2 diabetes mellitus, cardiovascular disease, inflammatory bowel disease, allergy, and certain types of cancer via low-grade inflammation. The inflammatory environment develops in the central nervous system, including the hypothalamus, and in the peripheral tissues, including the liver, adipose tissue, skeletal muscle, and intestine (Duan et al., 2018). In recent years, it has been revealed that HFD affects bone marrow (BM) components and hematopoietic stem cell (HSC) homeostasis through gut bacteria dysbiosis. For example, HFD loading alters the gut microbiota and changes the BM niche by increasing ectopic fat accumulation in BM, increasing fatty marrow via the activation of peroxisome proliferator-activated receptor γ2 (PPARγ2) and shifts HSCs toward granulocyte hematopoiesis (Luo et al., 2015). In addition, in *Spred1* knockout (KO) mice, abnormalities in the intestinal flora contribute to enhanced ERK signaling in HSCs, causing marked granulocyte hyperplasia, and this phenomenon is alleviated by depletion of the gut microbiota (Tadokoro et al., 2018). These dysbiosis-mediated abnormalities in the gut may be important for controlling low-grade inflammation via hematopoiesis, but the detailed mechanisms and regulators of the intestinal-blood cell association remain unclear.

The suppressors of cytokine signaling (SOCS) family is required to prevent spontaneous inflammation associated with excessive cytokine responses. The SOCS family contains eight proteins, SOCS1-7 and CIS (cytokine inducible SH2 containing protein), and is characterized by the presence of an SH2 domain that mediates interaction with signaling proteins, such as the JAK kinases and/or cytokine receptors, and a C-terminal SOCS Box motif. Regulation of signaling by IL-6 and G-CSF by SOCS3 appears to be important in preventing inflammation (Croker et al., 2003, 2004). Furthermore, SOCS3 is strongly associated with obesity and insulin resistance. Inhibition of SOCS3 in obese mice improves insulin sensitivity and fatty liver, and it also normalizes the increased expression of sterol regulatory element binding protein (SREBP)-1c, which is the key regulator of fatty acid synthesis in the liver (Ueki et al., 2004). These findings indicate that the inhibition of SOCS3 is a promising therapeutic target for improving glucose tolerance and HFD-induced inflammatory effects.

[1]Department of Hematology, Endocrinology and Metabolism, Faculty of Medicine, Niigata University, Niigata, Niigata 951-8510, Japan

[2]Department of Transfusion Medicine, Cell Therapy and Regenerative Medicine, Niigata University Medical and Dental Hospital, 1-754 Asahimachi-dori, Chuo-ku, Niigata, Niigata 951-8520, Japan

[3]Department of Endocrinology and Metabolism, Faculty of Medicine, University of Tsukuba, Tsukuba, Ibaraki 305-8575, Japan

[4]Histopathology Core Facility, Faculty of Medicine, Niigata University, Niigata, Niigata 951-8510, Japan

[5]Division of Molecular and Diagnostic Pathology, Niigata University Graduate School of Medical and Dental Sciences, Niigata, Niigata 951-8510, Japan

[6]Department of Cardiovascular Biology and Medicine, Juntendo University Graduate School of Medicine, Bunkyo-ku, Tokyo 113-8421, Japan

[7]Division of Bioinformatics, Niigata University Graduate School of Medical and Dental Sciences, Niigata, Niigata 951-8510, Japan

[8]Division of Complex Biosystem Research, Department of Research and Development, Institute of Natural Medicine, University of Toyama, Toyama, Toyama 930-0194, Japan

[9]Department of Clinical Laboratory Medicine, Kyoto University Hospital, Kyoto, Kyoto 606-8507, Japan

[10]Laboratory of Stem Cell Regulation, School of Life Sciences, Tokyo University of

Herein, we show systemic homozygous SOCS3 KO results in marked myeloid hematopoiesis and lethal inflammation under conditions of HFD loading. In these mice, myeloid cells invaded the liver and eventually caused systemic inflammation; however, inflammation was substantially improved by depletion of the gut microbiota using antibiotics.

RESULTS

Generation of mice lacking SOCS3 on the HFD diet

Complete SOCS3 deficiency in mice causes embryonic lethality due to the uncontrolled actions of leukemia inhibitory factor signaling (Roberts et al., 2001). To overcome the embryonic lethality of SOCS3 deficiency, we used a tamoxifen-inducible Cre-recombinase, *Rosa26-CreERT2* in combination with a homozygous floxed SOCS3 allele (*Socs3fl/fl*). To investigate the significant roles of SOCS3 in HFD, *Socs3*-KO genotypes were generated by treatment with tamoxifen. To explore the combined effect of both SOCS3 deficiency and HFD-load in inflammation, mice were established as indicated: SOCS3 deficiency in mice on HFD diet (*S3-HFD*, tamoxifen-treated *Socs3fl/fl*; *Rosa26-CreERT2*) or control chow (*S3-chow*, tamoxifen-treated *Socs3fl/fl*; *Rosa26-CreERT2*); functionally normal SOCS3 on HFD diet (*WT-HFD*, vehicle-treated *Socs3fl/fl*; *Rosa26-CreERT2*) or on control chow (*WT-chow*, vehicle-treated *Socs3fl/fl*; *Rosa26-CreERT2*) (Figure S1). Previously, we confirmed highly efficient Cre-ERT2-dependent recombination of the floxed *Socs3* allele in the hematopoietic organs of tamoxifen-, but not vehicle-treated mice, using Southern blotting (Ushiki et al., 2016). Near-complete tamoxifen-induced inactivation of the *Socs3* allele was also confirmed in the trunk of *Socs3* deficient mice, but not in intracranial organs, using genomic PCR (Figure S2).

SOCS3KO protected against diet-induced obesity and fatty liver and improved blood glucose concentration without increasing activity and energy metabolism

The S3-chow mice were lighter than WT-chow mice at 28 weeks of age. Furthermore, mice fed the HFD (WT-HFD) developed obesity; however, S3-HFD mice were significantly protected from diet-induced obesity. Thus, SOCS3KO restricts weight gain, especially that caused by HFD (Figure 1A). As for food intake at 15 weeks of age, intake (g/day) did not differ with HFD. Caloric intake (kcal/day) in WT-HFD was significantly higher than that in WT-chow, and the same was observed in S3-HFD compared with that in S3-chow. However, the intake (kcal/day) in WT-HFD and S3-HFD did not differ significantly (Figure 1B). Lipid intake (g/day) displayed the same trend as caloric intake. A significant increase between chow and HFD was evident in both WT and SOCS3-deficient models (Figure 1C). Therefore, the amount of food and the nutritional value of the food ingested cannot explain the significant weight difference observed between WT and SOCS3-deficient mice on the HFD. In parallel with the body weight change, the development of fatty liver and secretion of liver triglyceride (TG) were suppressed in S3-HFD mice on day 30 after tamoxifen treatment (Figures 1D and 1E) and myeloid infiltrations were observed in SOCS3-deficient mice (Figure 1D). Regarding movement, on day 30 after tamoxifen treatment, open field total distance was lower in the HFD group than in the control diet group in WT mice. The total distance was low in the chow group, and it did not change with HFD feeding in SOCS3-deficient mice (Figure 1F). The open field total movement duration agreed with the total distance trend observed (Figure 1G). The rotary momentum test revealed lower scores in WT-HFD mice than in normal diet. The scores of both SOCS3-deficient groups, HFD and normal diet, were lower than those of WT-chow mice on day 30 after tamoxifen treatment (Figure 1H). Respiratory exchange ratio appeared low in the HFD groups, for both WT and SOCS3-deficient mice, on day 30 after tamoxifen (Figure 1I). Blood glucose levels were higher in the WT-HFD group than in the S3-chow group, but there was no other difference (Figure 1J). Insulin resistance testing indicated lower blood glucose level in SOCS3KO mice than in WT mice on day 14 after tamoxifen treatment (Figure 1K), suggesting that the systemic effects of SOCS3-deficiency improved HFD-induced insulin resistance.

It has been reported that the circulating leptin concentration is higher in wild-type mice on an HFD than in mice on chow, whereas the leptin concentration in SOCS3 haploinsufficient mice on an HFD is not significantly higher than that in mice on chow (Howard et al., 2004). Consistent with this, the plasma leptin level was significantly increased by HFD in WT mice, and this was alleviated in S3 mice (Figure 1L).

Thus, SOCS3 deficiency ameliorated HFD-induced obesity and hepatic lipid secretion that cannot be attributed to improved metabolism and increased energy expenditure alone. In some cases, various types of tumors develop or are promoted in SOCS3-deficient mice including gastric and pancreatic cancer (Inagaki-Ohara et al., 2014; Lesina et al., 2011). These neoplasms were not detected on day 30 after tamoxifen in all phenotypes examined (Table S1). Thus, neoplasm is not associated with obesity resistance.

Pharmacy and Life Sciences, Hachioji, Tokyo 192-0392, Japan

[11]Blood Cells and Blood Cancer Division, the Walter and Eliza Hall Institute of Medical Research, Parkville, VIC 3052, Australia

[12]Department of Medical Biology, the University of Melbourne, Parkville, VIC 3052, Australia

[13]These authors contributed equally

[14]Lead contact

*Correspondence:
tushiki@med.niigata-u.ac.jp

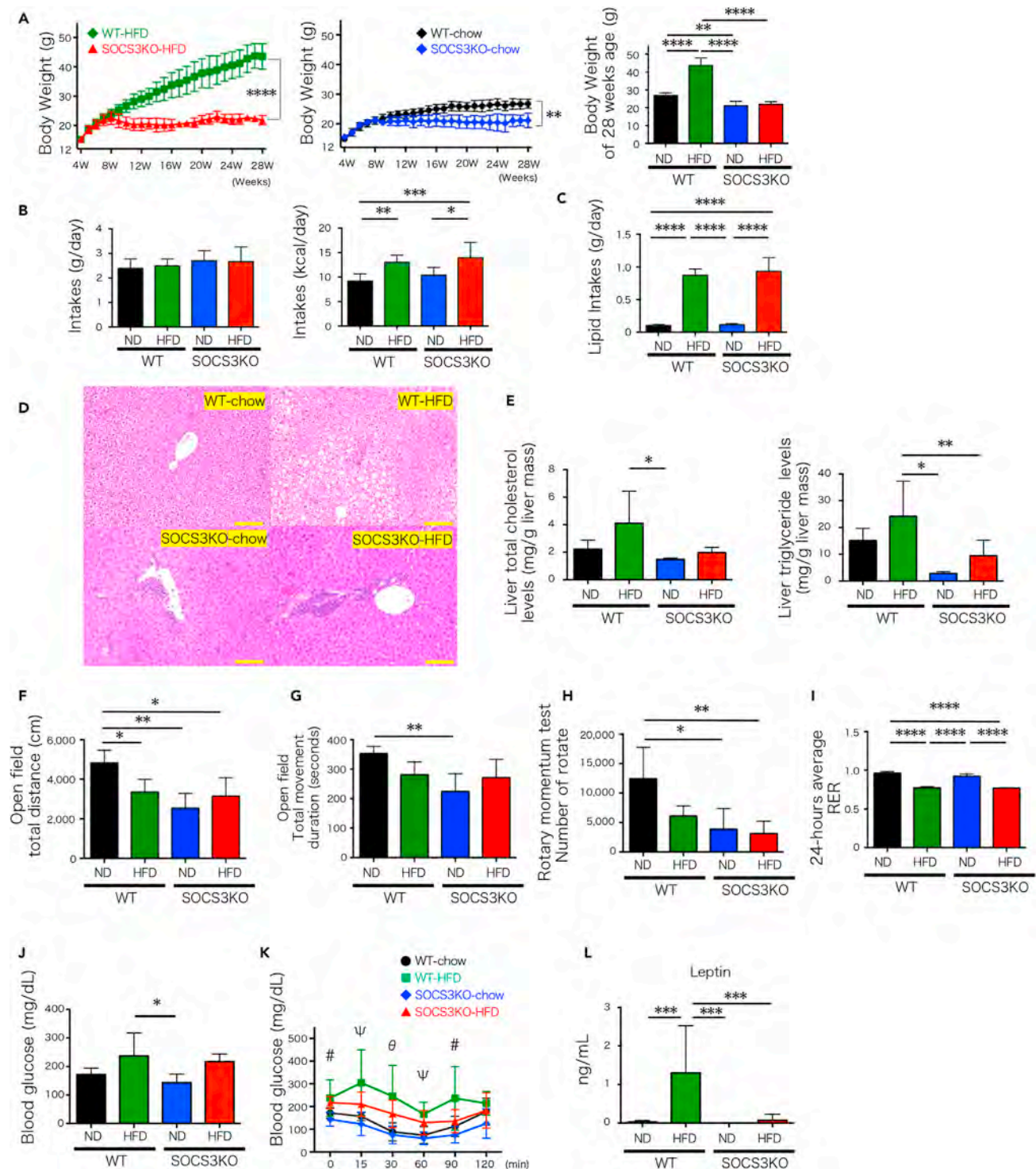https://doi.org/10.1016/j.isci.2021.103117

Figure 1. Effects of diet and genotype on body weight, liver fat, and glucose tolerance

(A) Weekly body weight gain. Mean ± SD is shown with ****$p < 0.0001$ and **$p < 0.01$ for the comparison of WT with HFD and S3 with HFD, or WT with chow and SOCS3KO with chow at 28 weeks after birth, using the one-way ANOVA with Tukey's multiple comparisons test, n = 3–22/group.

(B and C) Total daily food intake, total daily caloric intake, and lipid intake at 15 weeks of age, n = 6–9/group. Mean ± SD is shown with ****$p < 0.0001$, ***$p < 0.001$, **$p < 0.01$, and *$p < 0.05$.

(D) Liver pathology (hematoxylin and eosin staining).

SOCS3 deficiency combined with HFD induces rapid inflammatory disease with myeloid hematopoiesis

While SOCS3-deficiency improved obesity and fatty liver, the mice rapidly became unwell when fed the HFD from day 32 after tamoxifen treatment, and their median survival was 65.5 days after tamoxifen-induced deletion of SOCS3. In contrast, several S3-chow mice became moribund from day 106 after tamoxifen treatment; however, they did not reach 50% mean survival over a 6-month observation period. The control group mice (WT-chow, WT-HFD) did not become unwell (Figure 2A). All mice were analyzed upon initial signs of disease (hereinafter referred to as moribund). Inflammation was observed in the spleen and liver from day 30 after tamoxifen administration; thus, we defined this period as the pre-inflammation phase. Only S3-HFD mice showed marked neutrophilia in the blood (Figure 2B) and considerable splenomegaly (Figure 2C) in the pre-inflammation phase. Furthermore, S3-chow mice subsequently exhibited splenomegaly around the median survival time. Thus, SOCS3KO mice on a normal diet developed splenomegaly; however, spleen weight of these mice was significantly lower than that of the S3-HFD group and neutrophilia was not observed (Figures 2D and 2E). Thus, HFD is necessary to induce neutrophilia and more significant splenomegaly. Pathological analysis revealed that the S3-HFD group displayed hepatic inflammation without fatty liver in the pre-inflammation phase. Moribund S3-HFD mice often displayed inflammatory skin lesions such as pachyderma, alopecia, and/or ulcers (Figure 2F), and autopsies also revealed splenomegaly, lymphadenopathy, and inflammation in the liver, fat, lung, and kidney (Figure 2G). Thus, as SOCS3-deficient mice on normal chow or WT mice on the HFD did not display excessive granulopoiesis, the combination of SOCS3 deficiency and HFD induced rapid granulopoiesis from day 30 after tamoxifen treatment, suggesting that granulopoiesis contributed to systemic inflammation.

SOCS3 deficiency induced granulopoiesis in the spleen

Lymphoid follicle structure collapsed due to increasing numbers of CD11b$^+$Gr-1$^+$ granulocytes in the spleen (Figures 3A and 3B) under SOCS3 deficiency, but the percentage of granulocytes was significantly higher in the S3-HFD group than in the S3-chow group. Next, we investigated granulocyte maturation in the spleen in the pre-inflammation phase (Figure 3C). In brief, hematopoietic cells undergoing granulopoiesis were separated into subpopulations #1 to #5 by FACS analysis using c-Kit and Ly-6G markers, and granulocyte differentiation and maturation stages were classified as follows: subpopulation #1 comprised mainly myeloblasts, #2 contained an abundance of promyelocytes, #3 mainly myelocytes, #4 mainly metamyelocytes, and #5 mainly band cells and segmented cells. Cells undergoing granulocytic maturation (#4-#5) were predominant in SOCS3KO mice on both normal chow and HFD (Figure 3D). In addition, considering the extensive splenomegaly in S3-HFD, mature granulopoiesis is likely more active in the S3-HFD group than the S3-chow group. Colony assays revealed increased myeloid progenitor cells (CFU-GM, CFU-G, and CFU-M) in the spleen in SOCS3-deficient mice, with the HFD driving higher numbers of myeloid progenitor colonies in S3-HFD mice (Figure 3E). Thus, SOCS3 deficiency enhanced granulopoiesis without HFD in the spleen and maturation of granulocytes was similar in the S3-chow and S3-HFD groups. However, hematopoiesis indicated by myeloid progenitor cell number was significantly higher in the S3-HFD group than in the S3-chow group.

SOCS3 deficiency with HFD feeding accelerates hepatic inflammation without obesity and ectopic fat accumulation

SOCS3 deficiency improved HFD-induced obesity and ectopic fat accumulation (Figures 1A and 1E); however, myeloid infiltration was observed in the liver. These myeloid cells were observed in the entire liver, including the hepatic vein area, portal region, and liver parenchyma on day 30 after tamoxifen treatment during the pre-inflammation phase (Figure 4A). Additionally, analysis was performed on day 14 post-tamoxifen treatment, but at this time hepatic infiltration and splenomegaly were not observed, and in the serum, liver enzyme activities did not differ among the groups. The total cholesterol level was higher
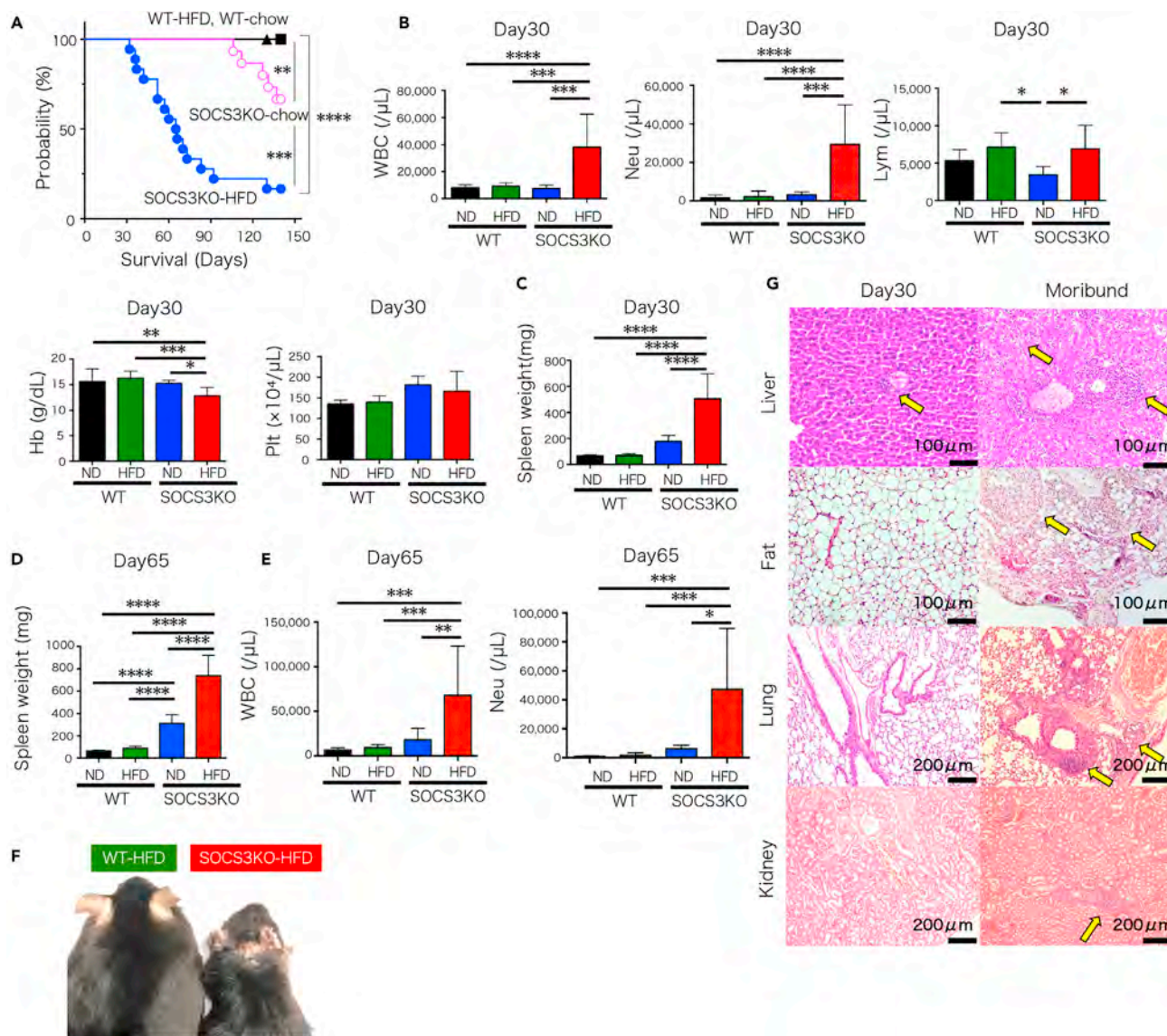
Figure 2. SOCS3KO exacerbates rapid granulopoiesis with HFD in the blood and spleen

(A) Disease onset in mice with systemic SOCS3KO. ****p < 0.0001, ***p < 0.001, and **p < 0.01 for the pairwise comparison of survival of S3-HFD (○) and S3-chow (●) or other control genotypes. Mantel-Cox Log rank test, n = 15–28/group.

(B and C) (B) Peripheral blood counts and (C) spleen weight on day 30 following tamoxifen or vehicle administration, n = 6–15.

(D and E) (D) Spleen weight and (E) peripheral blood cell counts on day 65 following tamoxifen or vehicle administration, n = 4–13/group.

(F) Images of representative live WT-HFD and S3-HFD mice on day 30 following tamoxifen or vehicle administration.

(G) Pathology in SOCS3-deficient mice on HFD. S3-HFD mice started to show liver inflammation on day 30 after tamoxifen administration (left column), but infiltration of inflammatory cells was not observed in fat, lung, and kidney. Moribund S3-HFD mice showed obvious infiltration of inflammatory cells (right column). Arrows indicate infiltrating inflammatory cells. Mean ± SD is shown with *p < 0.05, **p < 0.01, ***p < 0.001, and ****p < 0.0001 for comparison.

in the S3-HFD and WT-HFD groups than in the S3-chow and WT-chow groups (Figure 4B). In the pre-inflammatory phase (day 30 after tamoxifen treatment), the inflammation marker TNF-α was increased in the liver, but IL-6 in the S3-HFD group did not mirror this trend. Unexpectedly, marked Ly6G RNA expression was observed in the S3-HFD group, indicating excess neutrophil infiltration and blood cells in the liver as local inflammation (Figure 4C). Furthermore, elevation in CD11b, CD14, and CD68 RNA expression indicated monocyte and macrophage infiltration in the liver in the S3-HFD group. Although inflammasome markers IL-1β and Caspase-1 were not increased in the pre-inflammation phase (Figure 4D) in all phenotypes (day 30 after tamoxifen treatment), these genes were significantly increased in the S3-HFD group in the moribund phase (day 65 post-tamoxifen treatment) (Figure 4E).
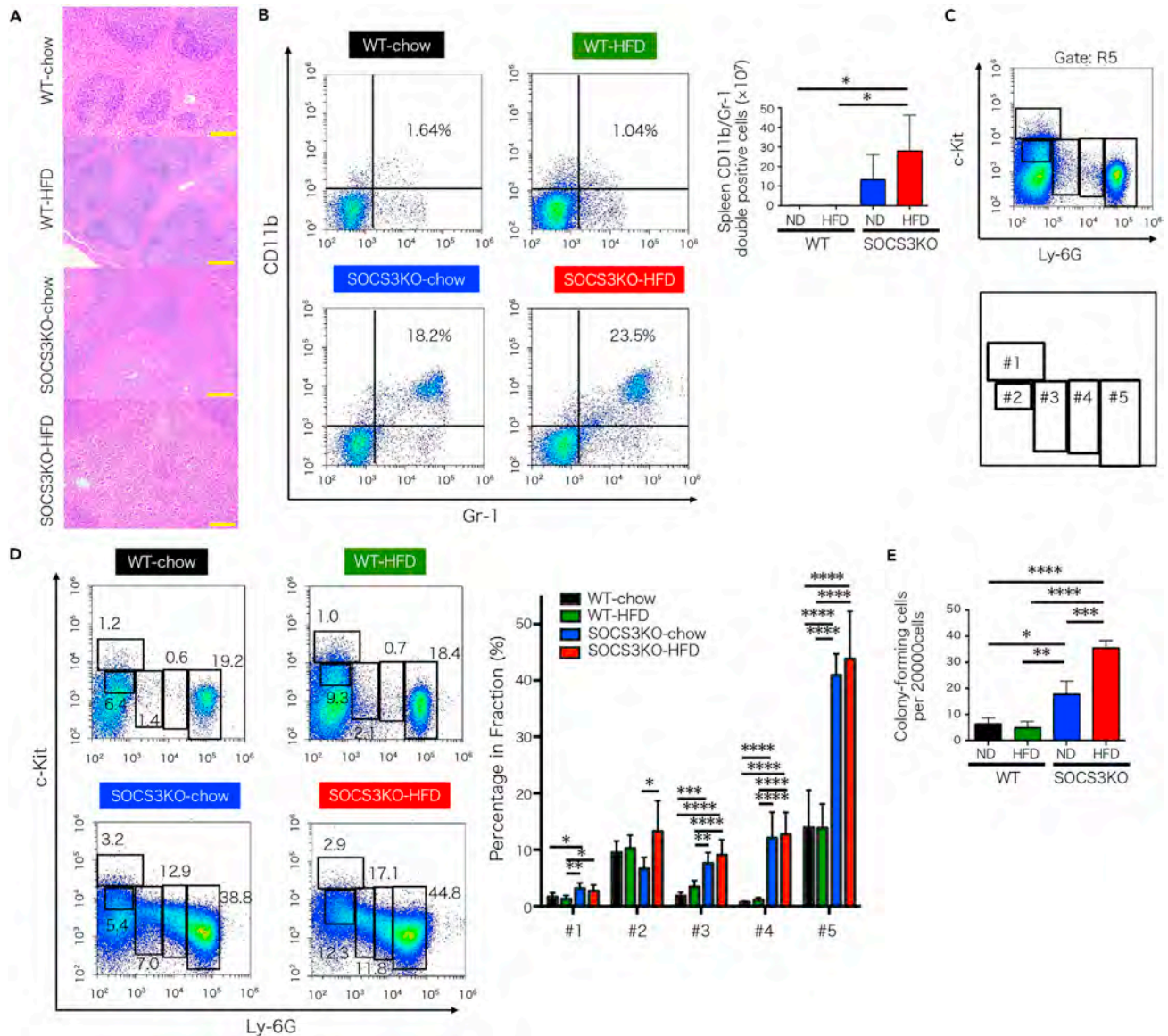
Figure 3. Characteristics of granulocytes and their maturation in the spleen

(A) Spleen pathology (hematoxylin and eosin stain) from mice with HFD on day 30 after tamoxifen treatment. Bar = 100 μm. n = 8–12/group.

(B) Granulocytes (CD11b$^+$Gr-1$^+$ cells) in the spleen on day 30 following tamoxifen or vehicle treatment, n = 3–7/group.

(C) After flow cytometric analysis, granulocyte differentiation and maturation stages were classified from gates #1 to #5.

(D) Flow cytometric analysis of granulopoiesis from immature to mature stages in the spleen on day 30 after tamoxifen treatment. n = 5–8/group.

(E) Total colony number in MethoCult M3534 containing SCF, IL-3, and IL-6, n = 3/group. Mean ± SD is shown with *p < 0.05, **p < 0.01, ***p < 0.001, and ****p < 0.0001 for comparison.

Furthermore, fatty acid synthetase including, fatty acid desaturase 1 (FADS-1), stearoyl-CoA desaturase 1 (SCD-1), elongation of very long chain fatty acids 6 (Elovl6), and SREBP-1 were present in the pre-inflammation phase (Oishi et al., 2017). The results indicated that FADS-1 was elevated by the HFD in the WT-HFD group, but this increase was abolished in the absence of SOCS3. In addition, *SCD-1* expression was lower in the WT-HFD group than in the WT-chow group, and *SCD-1* expression was low in the SOCS3-deficient groups, irrespective of diet. As fatty acid synthetase *FADS-1* is classified as an anti-inflammatory gene (Gromovsky et al., 2018) and *SCD-1* is classified as an inflammatory gene (Liu et al., 2010), intra-hepatic environment cannot be predicted only by fatty acid synthetase in the S3-HFD group. Regarding fat synthesis, low expression of *FADS-1* and *SCD-1* suppressed fat synthesis in the liver. SREBP-1 and Elovl6 expression levels were unchanged across all phenotypes (Figure S3).
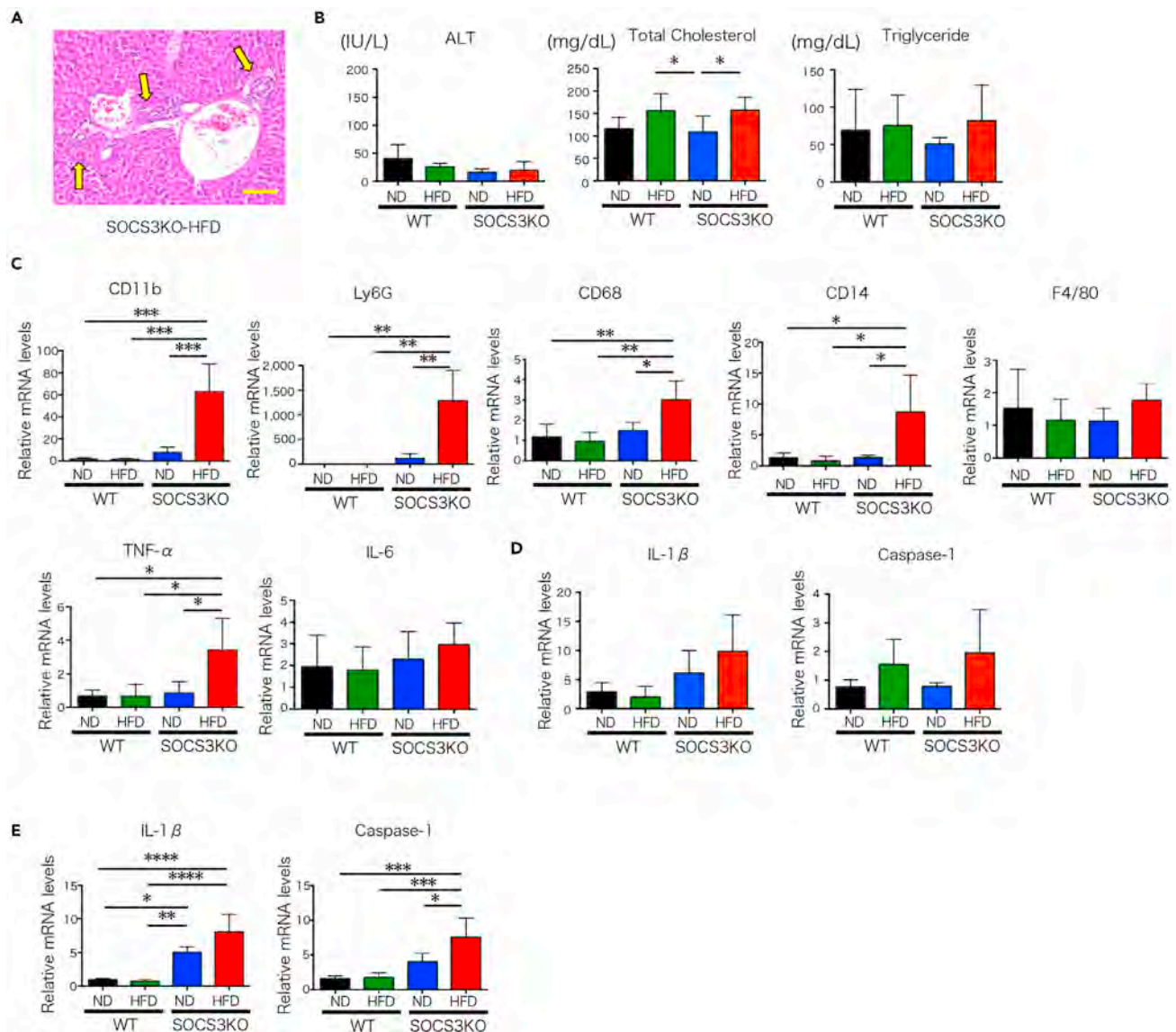
Figure 4. Features of inflammation and infiltration markers of myeloid series cells in the liver

(A) Photomicrograph showing inflammation and mixed hematopoietic infiltration of the liver in S3-HFD mice on day 30 following tamoxifen administration. Arrows indicate infiltrating inflammatory cells. Bar = 100μm.

(B) Biochemical examinations on day 30 following tamoxifen administration. n = 6–9/group.

(C) Inflammation markers: *TNF-α* and *IL-6* mRNA levels; Myeloid infiltration markers: *CD11b*, *F4/80*, *Ly6G*, and *CD68* mRNA levels. n = 3–6/group.

(D) Inflammasome markers: *IL-1β* and *Caspase-1* mRNA levels on day 30 following tamoxifen or vehicle administration. n = 3–4/group.

(E) Inflammasome markers on day 65 following tamoxifen or vehicle administration. n = 4–5/group. Mean ± SD is shown with *p < 0.05, **p < 0.01, ***p < 0.001, and ****p < 0.0001 for comparison, using the one-way ANOVA with Tukey's multiple comparisons test.

Hematopoietic SOCS3KO is not involved in HFD-induced inflammation and is not a direct pro-inflammatory factor

Given the excessive granulocyte infiltration into the liver, we next considered the specific role of hematopoietic loss of SOCS3. Mature myeloid-specific SOCS3KO mice (*LysM*; *LysMCre Socs3fl/fl*) were fed the HFD from 4 weeks of age. In *LysMCre Socs3fl/fl* mice, SOCS3 was partially deleted in peripheral white blood cells and intraperitoneal cells (Figure S4). While systemic lethal inflammation was not observed, HFD-induced obesity was present in mature myeloid-specific SOCS3KO mice on the HFD (Figures 5A and 5B). Myeloid-specific SOCS3KO mice exhibited mild HFD-induced fatty liver (Figure 5C); however SOCS3 deficiency showed there were trends of decrease in liver lipids in contrast to those in WT, thereby

A LysM-HFD, LysM-chow

S3-HFD

****

B LysM-HFD / LysM-chow

****

Body Weight of 28 weeks age (g)

**** **** **** ****

ND HFD ND HFD
WT   LysM

C WT-chow WT-HFD / LysM-chow LysM-HFD

D Liver total cholesterol levels (mg/g liver mass)

**

ND HFD ND HFD
WT   LysM

Liver triglyceride levels (mg/g liver mass)

** *

ND HFD ND HFD
WT   LysM

E LysM-chow / LysM-HFD

WBC (/μL)

ND HFD ND HFD
Day30   Day65

Neu (/μL)

LysM-chow / LysM-HFD

ND HFD ND HFD
Day30   Day65

F LysM-chow / LysM-HFD

Spleen weight (mg)

* *

ND HFD ND HFD
Day30   Day65

G WT-chow WT-HFD / Vav-chow Vav-HFD

H Liver total cholesterol levels (mg/g liver mass)

ND HFD ND HFD
WT   Vav

Liver triglyceride levels (mg/g liver mass)

ND HFD ND HFD
WT   Vav

I WBC (/μL)

ND HFD ND HFD
WT   Vav

Neu (/μL)

ND HFD ND HFD
WT   Vav

J Spleen weight (mg)

ND HFD ND HFD
WT   Vav

K WT-chow / WT-HFD / Vav-chow / Vav-HFD
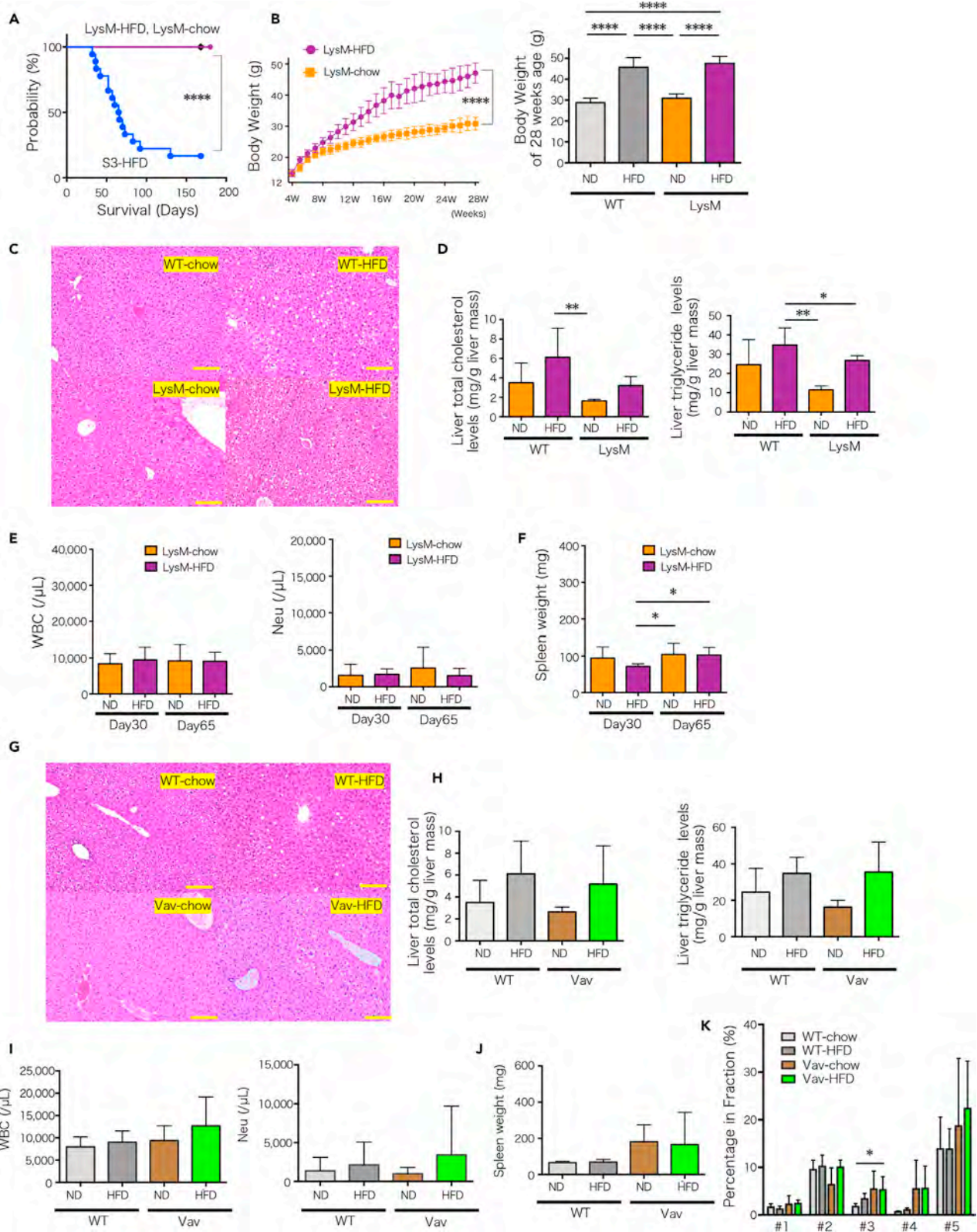
Percentage in Fraction (%)

*

#1 #2 #3 #4 #5

Figure 5. Effects of HFD diet on hematopoietic SOCS3-deficient mice

(A) Disease onset in mice with systemic SOCS3KO. ****p < 0.0001 for pairwise comparison of survival of S3-HFD (○), LysM-HFD (●), and LysM-chow (◆). Mantel-Cox Log rank test, n = 12–18 mice/group.

(B) Weekly body weight gain. Mean ± SD is shown with ****p < 0.0001 for comparison of LysM-chow and LysM-HFD, or WT with chow and WT with HFD at 28 weeks after birth, using the one-way ANOVA with Tukey's multiple comparisons test, n = 13–26/group.

(C and D) (C) Liver fat pathology (hematoxylin and eosin staining), (D) hepatic total cholesterol and triglyceride levels in LysM-SOCS3KO mice at 12 weeks of age, n = 5/group.

(E) Number of neutrophils in the blood at 30 days after HFD or chow intake, n = 7–11 in each group.

(F) Spleen weight, n = 5–9 in each group.

(G and H) (G) Liver fat pathology (hematoxylin and eosin staining), (H) hepatic total cholesterol and triglyceride levels in Vav-SOCS3KO mice at 12 weeks old, n = 5 in each group. Mean ± SD is shown with **p < 0.01, and *p < 0.05. Bar = 100µm.

(I) Numbers of neutrophils in the blood at 30 days in mice with hematopoietic SOCS3KO after HFD or chow intake, n = 3–12/group.

(J) Spleen weight, n = 3–12 in each group.

(K) Percentage of each fraction by flow cytometric analysis of murine granulopoiesis in the spleen at 30 days after tamoxifen administration. Mean ± SD is shown with *p < 0.05 and **p < 0.01 for comparison. LysM: mature myeloid-specific SOCS3KO mice, Vav: hematopoietic specific KO mice.

suppressing fatty liver in myeloid-specific SOCS3KO mice (Figure 5D). Inflammation was not observed in myeloid-specific SOCS3KO mice (Figure 5C). In addition, granulocytosis in peripheral blood and spleno-megaly were not observed (Figures 5E and 5F). Next, we investigated the effect of deletion of SOCS3 in the entire hematopoietic system, including myeloid progenitors, using Vav-cre (*VavCre Socs3fl/fl*). In *Vav-Cre Socs3fl/fl* mice, SOCS3 was completely deleted in peripheral white blood cells (Figure S4). The results in *VavCre Socs3fl/fl* mice were similar to those in *LysMCre Socs3fl/fl* mice: hepatic inflammation and excess neutrophilia-related systemic inflammation were not observed (Figures 5G and 5I). Hematopoietic-specific SOCS3KO mice displayed mild fatty liver (Figures 5G and 5H) but granulocytosis was not evident (Figures 5I and 5J). Differentiation and maturation of neutrophils in the spleen did not significantly differ between the *VavCre Socs3fl/fl* mice and controls (Figure 5K). These data suggest that the loss of SOCS3 in blood cells is not likely to be the cause of systemic inflammation, rather non-hematopoietic SOCS3 appears to be important.

Intestinal tract is the source of HFD-induced inflammation and depletion of the gut microbiota abolishes inflammation

Considering the above results, and given the link among diet, gut biota, and hematopoiesis as previously described (Luo et al., 2015; Tadokoro et al., 2018), a meta 16S rRNA gene sequencing analysis of intestinal microbiota was performed. The principal coordinate analysis showed genetic differences among micro-biota in all groups of mice (Figure 6A). Phylogenetic classification showed reduced *Bifidobacteriales* mem-bers in the HFD groups, including S3-HFD and WT-HFD. These were significantly altered by depletion of the gut microbiota with a cocktail of four antibiotics (4Abx, see STAR Methods) and phylogenetic classifi-cation indicated a dominance in *Lactobacillales* abundance in not only the HFD groups, but also the chow groups (Figure 6B). The survival of the S3-HFD group significantly improved following 4Abx treatment (Figure 6C). Thus, the intestinal tract was demonstrated as the primary inflammation-initiating organ. Inter-estingly, both granulopoiesis and splenomegaly were substantially reduced in the S3-HFD group (Figures 6D–6F), whereas there were no effects of 4Abx treatment on survival or granulopoiesis in WT mice. In addi-tion, altered granulocyte-maturation in the spleen was also significantly reduced by microbiota depletion in S3-HFD mice (Figure 6G). mRNA levels of *TNF-α* in the colon decreased across all phenotypes after microbiota depletion (Figure 6H). Therefore, depletion of the gut microbiota might also suppress colon inflammation by improving dysbiosis. The data suggest that SOCS3 plays a key role in controlling systemic inflammation caused by enteric bacteria in the context of an HFD.

Intestinal tract microbiota depletion improves myeloid hematopoiesis in S3-HFD mice

Next, we checked the serum cytokine/chemokine levels that could affect granulopoiesis and inflammation. Although the differences were not statistically significant, GM-CSF, IL-17A, CCL-2, and CCL-4 were higher in S3-HFD mice than in WT mice and normalized by the depletion of the gut microbiota. IL-6 and S100A8/A9 were higher in S3-chow than in WT, however compositions of gut microbiota such as *Bifidobacteriales* and *Clostridiales* are similar in S3-chow and WT-HFD, indicating SOCS3 deficiency itself potentially contributed to elevation of these cytokines. In addition, levels of these cytokines were reduced by the depletion of gut microbiota, indicating these cytokines were enhanced by gut microbiota-associated inflammation. Although, gene expression of TNF-α in the liver of S3-HFD mice was high (Figure 4), there were no differences in the serum protein levels (Figure 7A). Regarding the origin of IL-17A from Th17 cells,
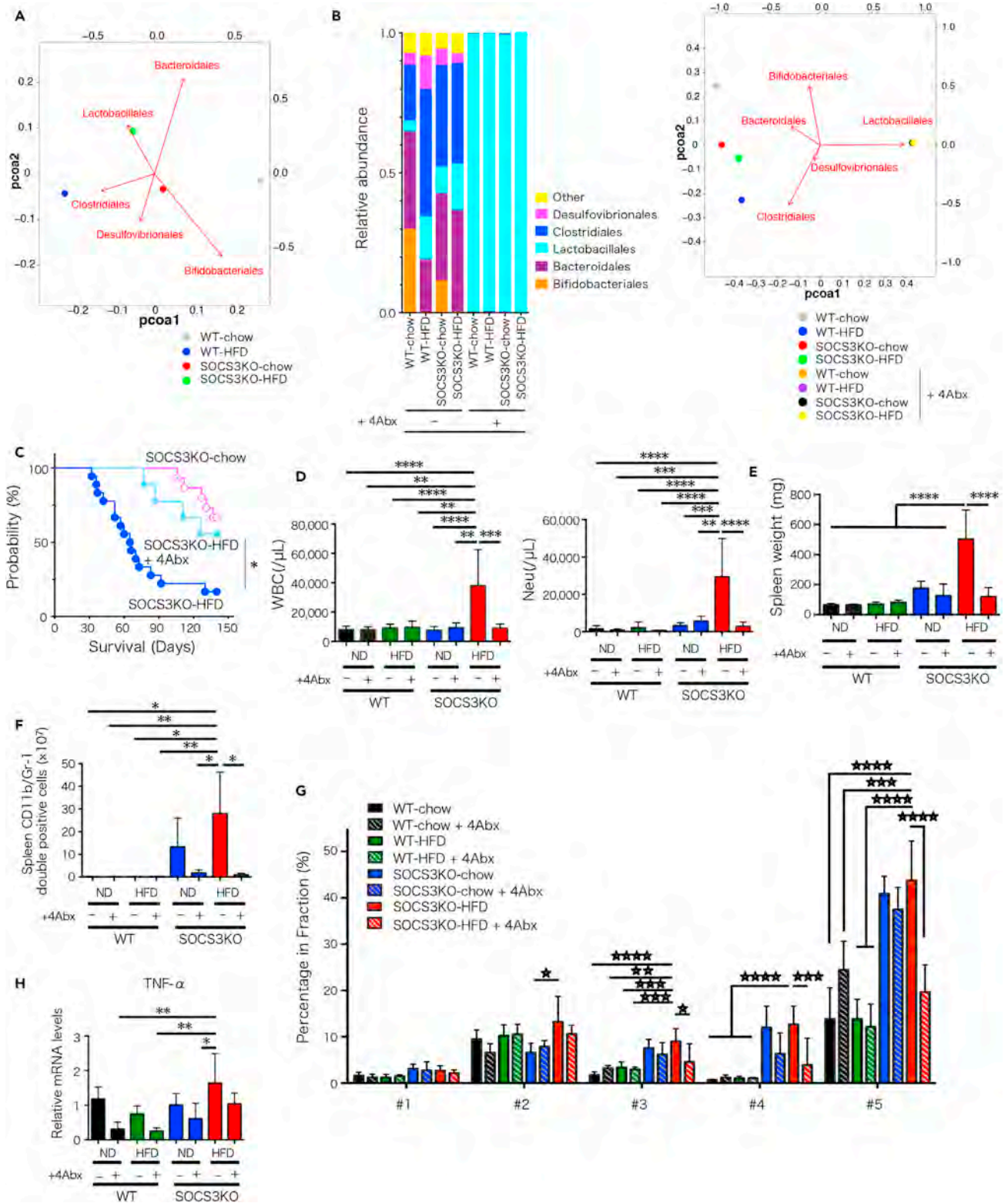
Figure 6. Effects of orally administered antibiotics for intestinal tract microbiota depletion

Cocktails containing four antibiotics (Abx) were administered from 4 weeks of age.

(A and B) (A) The results of the principal coordinate analysis and (B) relative mean abundance of the operative taxonomic units (OTUs) in the fecal matter at the order level. Proportions of the first (PCoA1) and second (PCoA2) components are shown (n = 3/group). Four Abx-treated (WT-chow, WT-HFD, S3-chow, and S3-HFD) and four dots overlap at one point.

(C) Disease onset in mice with SOCS3KO on HFD with four Abx (S3-HFD + 4Abx). Mantel-Cox Log rank test, n = 7–18 mice/group.

(D–F) (D) Number of neutrophils in the blood (n = 4–14), (E) spleen weight (n = 4–12) and (F) number of granulocytes (CD11b$^+$Gr-1$^+$ cells) in the spleen (n = 3–7) on day 30, following tamoxifen or vehicle treatment with or without 4Abx.

(G) Percentage of each murine granulopoiesis fraction, by flow cytometric analysis, in the spleen at 30 days after tamoxifen administration with or without 4Abx. n = 4–8/group. Mean ± SD is shown with *$p < 0.05$, **$p < 0.01$, ***$p < 0.001$, and ****$p < 0.0001$ for comparison of S3-HFD with all phenotypes.

(H) gut inflammation: *TNF-α* mRNA concentration in the colon on day 30 following tamoxifen administration with or without 4Abx. n = 3–4/group. Mean ± SD is shown with **$p < 0.05$, **$p < 0.01$, ***$p < 0.001$, and ****$p < 0.0001$ for comparison, One-way ANOVA with Tukey's multiple comparisons test. Four Abx; ampicillin, neomycin, metronidazole, and vancomycin.

which are abundant in the gut, especially the duodenum (Esplugues et al., 2011), we checked IL-17A- and IL-17-related genes in the duodenum. In addition, Th17 cells also express the chemokine receptor CCR6 in a cell-specific manner. However, there was no significant difference in the expression levels of IL-17A- and IL-17-related genes and CCR6 between WT and SOCS3-deficient mice in the duodenum before microbiota depletion (Figure S5). Regarding hematopoiesis in the BM, myeloid hyperplasia persisted in SOCS3-deficient mice with microbiota depletion (Table S1), and Gram staining revealed no bacteria in all groups (Table S2). In addition, HSCs (Lineage$^-$Sca-1$^+$c-Kit$^+$; LSK cells and CD34$^-$ LSK cells) and myeloid progenitors (common myeloid progenitor; CMP and granulocyte-macrophage progenitor; GMP) were significantly higher in S3-HFD mice than WT mice. However, these differences were variably alleviated by 4Abx treatment (Figure 7B). Combined with the observation that the elevated leukocyte count observed in S3-HFD mice was reversed by microbiota depletion, the existence of myeloproliferative diseases was unlikely in these mice.

DISCUSSION

Previously, systemic SOCS3 haploinsufficiency has been shown to attenuate diet-induced obesity by improving insulin resistance and enhancing leptin sensitivity (Howard et al., 2004). Thus, SOCS3KO is expected to improve obesity and obesity-associated metabolic complications. In fact, while aortic dissection is associated with arteriosclerosis or hypertension, smooth muscle specific SOCS3KO (Hirakata et al., 2020) or conversely SOCS3 expression in macrophages (Ohno-Urabe et al., 2018) protected against aortic dissection via inflammation control. However, systemic homogeneous SOCS3KO resulted in systemic inflammation due to excess myeloid hematopoiesis, particularly granulopoiesis. SOCS3 is reportedly associated with HFD-induced low-grade inflammation in local organs (Duan et al., 2018; Sachithanandan et al., 2010), however, obvious systemic inflammation and excess granulopoiesis has not been reported.

Systemic haploinsufficiency or neural cell-specific SOCS3KO was originally reported to enhance hypothalamic leptin signals and reduce weight gain in mice on an HFD (Howard et al., 2004; Mori et al., 2004). In our study, mice were fed an HFD to examine "systemic" homogeneous SOCS3KO effects on obesity. The results demonstrated that there were no differences in dietary intake across all genotypes, thus the amounts of consumed calories and fat intake were the same between the S3-HFD and WT-HFD groups. As tamoxifen cannot easily transit the blood–brain barrier, Cre recombinase cannot be efficiently released in the CreERT system in intracranial organs. In turn, this resulted in low SOCS3 deletion rates and presumably no accentuation of leptin signals in intracranial organs, including the hypothalamus. SOCS3KO mice on the HFD received high calories without increasing activity and energy consumption. In addition, the phenotype differed from brain-specific SOCS3KO mice (Mori et al., 2004), especially regarding appetite. Systemic inflammation was suspected to be strongly associated with obesity resistance in systemic SOCS3KO, rather than enhanced leptin signaling. In fact, the serum leptin level was not increased in SOCS3KO mice on the HFD.

Similar phenomena have been observed in organ-specific SOCS3KO mice. Liver-specific SOCS3KO mice exhibited improved insulin resistance on the control diet; however, liver-specific KO mice on the HFD exhibited increased hypothalamic SOCS3 expression and fatty acid synthase expression. Finally, liver-specific KO mice on the HFD displayed obesity and hepatic inflammation (Sachithanandan et al., 2010). In this study, hepatic inflammation was observed with an increase in F4/80-positive cells, and hepatic gene expression and plasma levels of TNF-α and IL-6 were also elevated, indicating that independent hepatic SOCS3KO can potentially induce low-grade inflammation. In our study, systemic SOCS3KO also showed
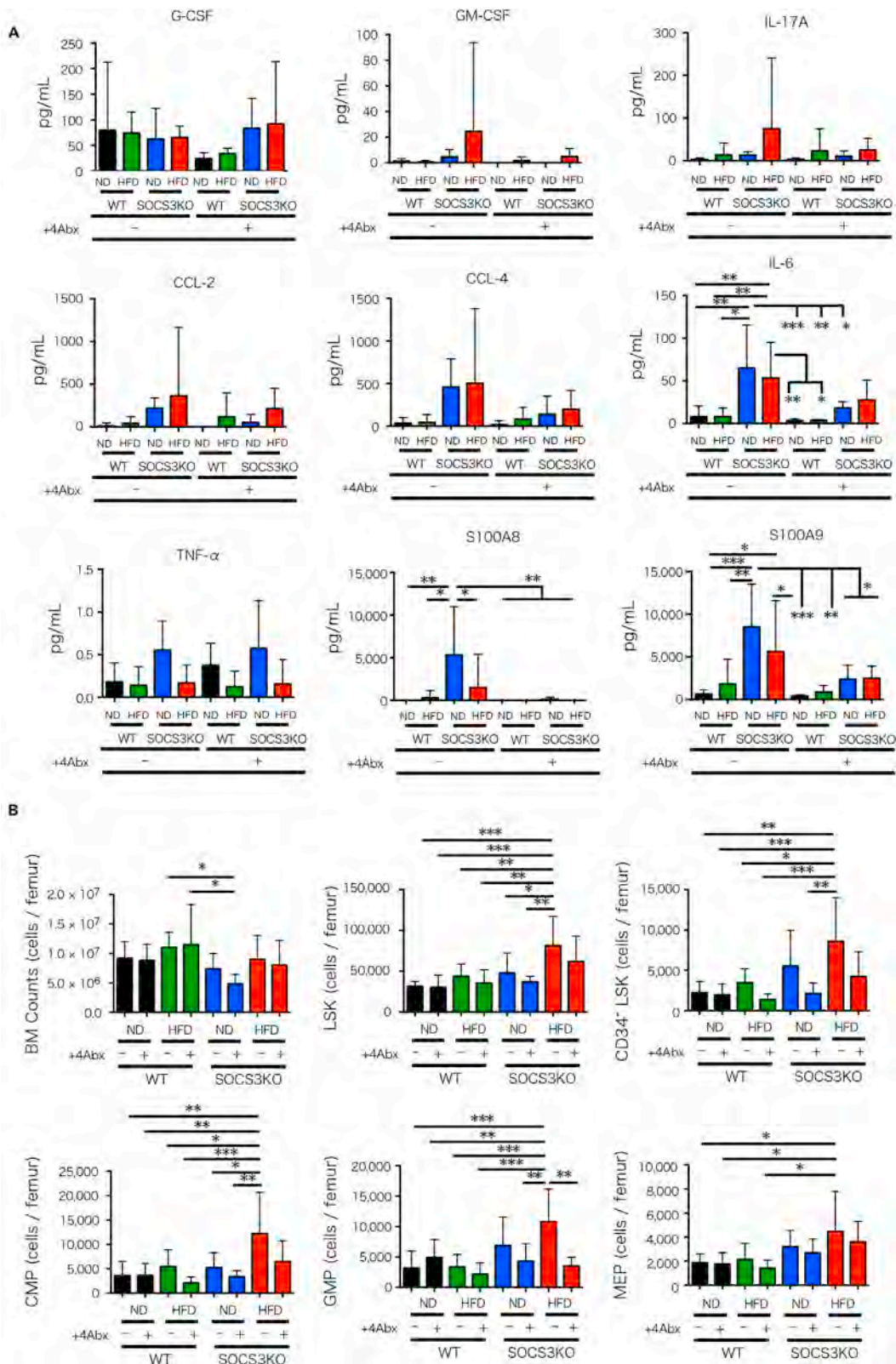
Figure 7. Effects of intestinal tract microbiota depletion on myeloid hematopoiesis

(A) Concentrations of cytokines/chemokines in the serum on day 30 following tamoxifen administration with or without 4Abx. n = 6–12/group.

(B) Absolute numbers of BM cells, Lineage−Sca-1+c-Kit+ (LSK) cells, CD34−LSK cells, CMP cells (Lineage−Sca-1−c-Kit+CD16/32LowCD34+), GMP cells (Lineage−Sca-1−c-Kit+CD16/32HighCD34+), MEP cells (Lineage−Sca-1−c-Kit+CD16/32−CD34−) in the femurs on day 30 following tamoxifen administration with or without 4Abx. n = 6–11/group. Mean ± SD is shown with *p < 0.05, **p < 0.01, and ***p < 0.001 for comparison using the one-way ANOVA with Tukey's multiple comparisons test.

low-grade inflammation similar to hepatic SOCS3KO; however, this inflammation was attenuated by the depletion of the gut microbiota. These phenomena indicated gut dysbiosis accelerated hepatic inflammation. Skeletal muscle-specific SOCS3KO mice displayed improved insulin resistance (Jorgensen et al., 2013). It has been confirmed that skeletal muscle damage in SOCS3KO mature muscle fibers did not improve muscle regeneration but tended to induce an inflammatory response with elevated TNF-α and macrophage infiltration in muscles (Swiderski et al., 2016).

As for fatty liver, here, systemic SOCS3 deficiency clearly improved fatty liver compared to that in wild-type mice on the HFD. The phosphorylation of STAT signal transducers is important against both inflammation and metabolism. For example, the level of IL-6 and phosphorylation of STAT3 signaling in hepatocytes are reported to change hepatic metabolism toward the suppression of hepatic glucose production (Inoue et al., 2006), or to improve fatty liver on a choline-deficient, ethionine-supplemented diet (Kroy et al., 2010). In our model, hepatic *IL-6* gene expression was not different, but serum IL-6 level was significantly elevated in SOCS3-deficient mice compared with that in wild-type mice in the Luminex assay. In addition, SOCS3 deficiency can result in prolonged phosphorylation of STAT3 signaling (Ushiki et al., 2016); thus, a high serum IL-6 level with SOCS3 deficiency might be one of the factors that contribute to improving fatty liver.

We previously demonstrated a rapid inflammation and neutrophilia in mice lacking both SOCS1 and SOCS3 in hematopoietic cells (Ushiki et al., 2016). We showed that SOCS1KO and SOCS3KO independently modulate the proliferation and activation of lymphoid and myeloid cells in the onset of rapid inflammatory disease. In brief, excessive CD8+ CD44hi T cells, a defining feature of the absence of SOCS1 (Cornish et al., 2003; Davey et al., 2005), were observed and increased auto-reactive CD8+ T cells underpins the autoimmunity in SOCS1-deficient mice (Davey et al., 2005). Our previous data were extended to this model to suggest that the absence of SOCS3, in the already pro-inflammatory environment established by SOCS1 deficiency, results in hyper-responsiveness of immune cells to cytokines, such as G-CSF and IL-6, even in modest amounts, and substantially accelerates myeloid proliferation and inflammatory infiltration of the target tissues (Ushiki et al., 2016). Thus, a lack of SOCS3 alone in hematopoietic cells did not result in disease development (Croker et al., 2012); however, SOCS3KO could accelerate inflammation via excessive granulopoiesis (Ushiki et al., 2016). Thus, regarding granulopoiesis in the current study, stimulation from activated T cell or low-grade inflammation by metabolic stress may be involved in granulocyte proliferation in SOCS3KO hematopoiesis. Our results suggest that GM-CSF, IL-17A, CCL-2, and CCL-4 are candidates as cytokines/chemokines that may contribute to systemic inflammation in S3-HFD mice and worthy of further study. As for IL-17A, SOCS3 is known to suppress Th17 differentiation (Chen et al., 2006; Qin et al., 2009), and Th17 cells are also known to be abundant in the gut (Esplugues et al., 2011). In our study, IL-17A and related gene expression in the duodenum of S3-HFD did not differ from those in other groups. Thus, IL-17 may be secreted from other organs that show local inflammation.

The effects of an HFD on hematopoiesis are also becoming apparent. HFD decreases the number of long-term LSK cells and shifts hematopoiesis from lymphoid to myeloid differentiation at the progenitor cell level (Luo et al., 2015). HFD also affects the bone marrow by altering the gut microbiota (Luo et al., 2015). In our experiments, myeloid cell-infiltration was observed in the spleen and liver in the S3-HFD group. However, this inflammation was not seen in myeloid-specific SOCS3KO mice. This indicates that excess myeloid hematopoiesis in the S3-HFD group requires the involvement of intestinal and hepatic inflammation, rather than the direct effects of HFD or SOCS3 deficiency on blood cells. In fact, LSK and myeloid progenitors indicated shifts to myeloid differentiation from the HSC-level in S3-HFD mice in our study. BM histopathology also showed myeloid hyperplasia, slight erythroid hypoplasia, and megakaryocytosis features resembling chronic myeloid leukemia feature. However, myeloid hematopoiesis was significantly reduced in the BM and peripheral blood in response to depletion of the gut microbiota, indicating that myeloid proliferation was reversible and likely to have a crucial role in the systemic inflammation development in S3-deficient mice on the HFD.

Suppression of the gut microbiota substantially alleviated myeloid hematopoiesis and halted the progression of systemic inflammation in S3-HFD mice. In addition, the gut microbiota composition was altered by antibiotic treatment to primarily enrich *Lactobacillales* in all groups. It has been reported that HFD chronically increased plasma bacterial lipopolysaccharide (LPS) levels by increasing the proportion of LPS-containing microbiota in the gut, called metabolic endotoxemia. In our study, *Bifidobacteriales* members were reduced in the HFD groups (Turnbaugh et al., 2006). Bifidobacteria are known to reduce intestinal LPS levels and improve mucosal barrier function (Cani et al., 2007b). Thus, the HFD groups are suspected to be sensitive to HFD-induced low-grade inflammation. Furthermore, various myeloid cells, such as granulocytes, monocytes, and macrophages, infiltrated the liver due to HFD-induced metabolic stress in our study. LPS receptor CD14-mutant mice on an HFD did not exhibit inflammation in the adipose tissue and liver, whereas insulin sensitivity was improved (Cani et al., 2007a). This suggests that CD14 cells in S3-HFD mice might enhance metabolic endotoxemia. It has also been shown that bacteria belonging to *Clostridiales* can induce Treg differentiation (Atarashi et al., 2011; Furusawa et al., 2013). We showed that SOCS3KO mice on an HFD displayed a slight decrease in *Clostridiales* in contrast to WT mice on an HFD. Thus, dysbiosis could affect the pro-inflammatory environment in SOCS3KO mice on an HFD.

In conclusion, SOCS3 is strongly associated with excess myeloid hematopoiesis in the context of the HFD. SOCS3 deficiency may cause resistance to diet-induced obesity but also causes severe systemic inflammation accompanying HFD-induced microbiota alteration. Therefore, although SOCS3 could be a therapeutic target for obesity, potent inflammatory adverse reaction should be taken into account.

Limitations of the study

This study shows that systemic deletion of SOCS3 results in excessive myeloid hematopoiesis and hepatic inflammation, which are dependent on gut microbiota. Moreover, SOCS3 crucially regulates intestinal dysbiosis-mediated inflammation with HFD. However, it is currently unclear how a HFD can alter the composition of the gut microbiota. Similarly, future studies will further define the specific roles of SOCS3 in regulation of the gut microbiota and systemic inflammation in this context.

STAR★METHODS

Detailed methods are provided in the online version of this paper and include the following:

- KEY RESOURCES TABLE
- RESOURCE AVAILABILITY
  - Lead contact
  - Materials availability
  - Data and code availability
- EXPERIMENTAL MODEL AND SUBJECT DETAILS
  - Animals and ethics statement
- METHOD DETAILS
  - Tamoxifen treatment and genotyping
  - High fat diet
  - Antibiotics treatment
  - Blood glucose measurement
  - Hepatic lipid analysis
  - Hematology and flow cytometry
  - Colony assay
  - RT-PCR analysis
  - Cytokine Luminex assay
  - Physiological analyses
  - Bacterial 16S rRNA amplicon sequencing and analysis
- QUANTIFICATION AND STATISTICAL ANALYSIS

SUPPLEMENTAL INFORMATION

Supplemental information can be found online at https://doi.org/10.1016/j.isci.2021.103117.

AUTHOR CONTRIBUTIONS

K.C. and T.U. designed all studies and wrote the manuscript. K.C., T.U., and H.I. performed most of the experiments. S.T., T.S., T.K., and M.M. performed FACS analyses. H.I. and M.A. performed hepatic lipid analyses. K.C., H.I., R.O., and Y.A. performed pathological analyses. I.S. analyzed physiological analyses data. T.U. and H.H. provided advice regarding granulopoiesis. T.U. and S.O. analyzed bioinformatic data. T.U., M.W., Y.F., Y.N., H.H., and W.A. reviewed and edited the paper. T.U., Y.N., W.A., H.S., and H.S. provided information regarding all experiments.

DECLARATION OF INTERESTS

The authors declare no competing interests.

REFERENCES

Anastassiadis, K., Glaser, S., Kranz, A., Berhardt, K., and Stewart, A.F. (2010). A practical summary of site-specific recombination, conditional mutagenesis, and tamoxifen induction of CreERT2. Methods Enzymol. 477, 109–123.

Atarashi, K., Tanoue, T., Shima, T., Imaoka, A., Kuwahara, T., Momose, Y., Cheng, G., Yamasaki, S., Saito, T., Ohba, Y., et al. (2011). Induction of colonic regulatory T cells by indigenous Clostridium species. Science 331, 337–341.

Cani, P.D., Amar, J., Iglesias, M.A., Poggi, M., Knauf, C., Bastelica, D., Neyrinck, A.M., Fava, F., Tuohy, K.M., Chabo, C., et al. (2007a). Metabolic endotoxemia initiates obesity and insulin resistance. Diabetes 56, 1761–1772.

Cani, P.D., Neyrinck, A.M., Fava, F., Knauf, C., Burcelin, R.G., Tuohy, K.M., Gibson, G.R., and Delzenne, N.M. (2007b). Selective increases of bifidobacteria in gut microflora improve high-fat-diet-induced diabetes in mice through a mechanism associated with endotoxaemia. Diabetologia 50, 2374–2383.

Caporaso, J.G., Lauber, C.L., Walters, W.A., Berg-Lyons, D., Lozupone, C.A., Turnbaugh, P.J., Fierer, N., and Knight, R. (2011). Global patterns of 16S rRNA diversity at a depth of millions of sequences per sample. Proc. Natl. Acad. Sci. U S A 108, 4516–4522.

Chen, Z., Laurence, A., Kanno, Y., Pacher-Zavisin, M., Zhu, B.M., Tato, C., Yoshimura, A., Hennighausen, L., and O'Shea, J.J. (2006). Selective regulatory function of Socs3 in the formation of IL-17-secreting T cells. Proc. Natl. Acad. Sci. U S A 103, 8137–8142.

Clausen, B.E., Burkhardt, C., Reith, W., Renkawitz, R., and Forster, I. (1999). Conditional gene targeting in macrophages and granulocytes using LysMcre mice. Transgenic Res. 8, 265–277.

Cornish, A.L., Davey, G.M., Metcalf, D., Purton, J.F., Corbin, J.E., Greenhalgh, C.J., Darwiche, R., Wu, L., Nicola, N.A., Godfrey, D.I., et al. (2003). Suppressor of cytokine signaling-1 has IFN-gamma-independent actions in T cell homeostasis. J. Immunol. 170, 878–886.

Croker, B.A., Kiu, H., Pellegrini, M., Toe, J., Preston, S., Metcalf, D., O'Donnell, J.A., Cengia, L.H., McArthur, K., Nicola, N.A., et al. (2012). IL-6 promotes acute and chronic inflammatory disease in the absence of SOCS3. Immunol. Cell Biol. 90, 124–129.

Croker, B.A., Krebs, D.L., Zhang, J.G., Wormald, S., Willson, T.A., Stanley, E.G., Robb, L., Greenhalgh, C.J., Forster, I., Clausen, B.E., et al. (2003). SOCS3 negatively regulates IL-6 signaling in vivo. Nat. Immunol. 4, 540–545.

Croker, B.A., Metcalf, D., Robb, L., Wei, W., Mifsud, S., DiRago, L., Cluse, L.A., Sutherland, K.D., Hartley, L., Williams, E., et al. (2004). SOCS3 is a critical physiological negative regulator of G-CSF signaling and emergency granulopoiesis. Immunity 20, 153–165.

Davey, G.M., Starr, R., Cornish, A.L., Burghardt, J.T., Alexander, W.S., Carbone, F.R., Surh, C.D., and Heath, W.R. (2005). SOCS-1 regulates IL-15-driven homeostatic proliferation of antigen-naive CD8 T cells, limiting their autoimmune potential. J. Exp. Med. 202, 1099–1108.

Duan, Y., Zeng, L., Zheng, C., Song, B., Li, F., Kong, X., and Xu, K. (2018). Inflammatory links between high fat diets and diseases. Front. Immunol. 9, 2649.

Esplugues, E., Huber, S., Gagliani, N., Hauser, A.E., Town, T., Wan, Y.Y., O'Connor, W., Jr., Rongvaux, A., Van Rooijen, N., Haberman, A.M., et al. (2011). Control of TH17 cells occurs in the small intestine. Nature 475, 514–518.

Furusawa, Y., Obata, Y., Fukuda, S., Endo, T.A., Nakato, G., Takahashi, D., Nakanishi, Y., Uetake, C., Kato, K., Kato, T., et al. (2013). Commensal microbe-derived butyrate induces the differentiation of colonic regulatory T cells. Nature 504, 446–450.

Gromovsky, A.D., Schugar, R.C., Brown, A.L., Helsley, R.N., Burrows, A.C., Ferguson, D., Zhang, R., Sansbury, B.E., Lee, R.G., Morton, R.E., et al. (2018). Delta-5 fatty acid desaturase FADS1 impacts metabolic disease by balancing proinflammatory and proresolving lipid mediators. Arterioscler. Thromb. Vasc. Biol. 38, 218–231.

Hirakata, S., Aoki, H., Ohno-Urabe, S., Nishihara, M., Furusho, A., Nishida, N., Ito, S., Hayashi, M., Yasukawa, H., Imaizumi, T., et al. (2020). Genetic deletion of Socs3 in smooth muscle cells ameliorates aortic dissection in mice. JACC Basic Transl. Sci. 5, 126–144.

Howard, J.K., Cave, B.J., Oksanen, L.J., Tzameli, I., Bjorbaek, C., and Flier, J.S. (2004). Enhanced leptin sensitivity and attenuation of diet-induced obesity in mice with haploinsufficiency of Socs3. Nat. Med. 10, 734–738.

Inagaki-Ohara, K., Mayuzumi, H., Kato, S., Minokoshi, Y., Otsubo, T., Kawamura, Y.I., Dohi, T., Matsuzaki, G., and Yoshimura, A. (2014). Enhancement of leptin receptor signaling by SOCS3 deficiency induces development of gastric tumors in mice. Oncogene 33, 74–84.

Inoue, H., Ogawa, W., Asakawa, A., Okamoto, Y., Nishizawa, A., Matsumoto, M., Teshigawara, K., Matsuki, Y., Watanabe, E., Hiramatsu, R., et al. (2006). Role of hepatic STAT3 in brain-insulin action on hepatic glucose production. Cell Metab. 3, 267–275.

Jorgensen, S.B., O'Neill, H.M., Sylow, L., Honeyman, J., Hewitt, K.A., Palanivel, R., Fullerton, M.D., Oberg, L., Balendran, A., Galic, S., et al. (2013). Deletion of skeletal muscle SOCS3 prevents insulin resistance in obesity. Diabetes 62, 56–64.

Joseph, C., Quach, J.M., Walkley, C.R., Lane, S.W., Lo Celso, C., and Purton, L.E. (2013). Deciphering hematopoietic stem cells in their niches: a critical appraisal of genetic models, lineage tracing, and imaging strategies. Cell Stem Cell 13, 520–533.

Katagiri, T., Uemura, S., Ushiki, T., Nakajima-Takagi, Y., Oshima, M., Mikami, T., Kawasaki, A., Ishiguro, H., Tanaka, T., Sone, H., et al. (2021). Distinct effects of chondroitin sulfate on hematopoietic cells and the stromal microenvironment in bone marrow hematopoiesis. Exp. Hematol. 96, 52–62.e55.

Kiu, H., Hilton, D.J., Nicola, N.A., Ernst, M., Marquez, R., Alexander, W.S., Roberts, A.W., and McManus, E.J. (2007). Mechanism of crosstalk inhibition of IL-6 signaling in response to LPS and TNFalpha. Growth Factors 25, 319–328.

Kroy, D.C., Beraza, N., Tschaharganeh, D.F., Sander, L.E., Erschfeld, S., Giebeler, A., Liedtke, C., Wasmuth, H.E., Trautwein, C., and Streetz, K.L. (2010). Lack of interleukin-6/glycoprotein 130/signal transducers and activators of transcription-3 signaling in hepatocytes predisposes to liver steatosis and injury in mice. Hepatology 51, 463–473.

Kuba, M., Matsuzaka, T., Matsumori, R., Saito, R., Kaga, N., Taka, H., Ikehata, K., Okada, N., Kikuchi, T., Ohno, H., et al. (2015). Absence of Elovl6 attenuates steatohepatitis but promotes gallstone formation in a lithogenic diet-fed Ldlr(-/-) mouse model. Sci. Rep. 5, 17604.

Lesina, M., Kurkowski, M.U., Ludes, K., Rose-John, S., Treiber, M., Klöppel, G., Yoshimura, A., Reindl, W., Sipos, B., Akira, S., et al. (2011). Stat3/Socs3 activation by IL-6 transsignaling promotes progression of pancreatic intraepithelial neoplasia and development of pancreatic cancer. Cancer Cell 19, 456–469.

Liu, X., Miyazaki, M., Flowers, M.T., Sampath, H., Zhao, M., Chu, K., Paton, C.M., Joo, D.S., and Ntambi, J.M. (2010). Loss of Stearoyl-CoA desaturase-1 attenuates adipocyte inflammation: effects of adipocyte-derived oleate. Arterioscler. Thromb. Vasc. Biol. 30, 31–38.

Luo, Y., Chen, G.L., Hannemann, N., Ipseiz, N., Kronke, G., Bauerle, T., Munos, L., Wirtz, S., Schett, G., and Bozec, A. (2015). Microbiota from obese mice regulate hematopoietic stem cell differentiation by altering the bone niche. Cell Metab. 22, 886–894.

Mori, H., Hanada, R., Hanada, T., Aki, D., Mashima, R., Nishinakamura, H., Torisu, T., Chien, K.R., Yasukawa, H., and Yoshimura, A. (2004). Socs3 deficiency in the brain elevates leptin sensitivity and confers resistance to diet-induced obesity. Nat. Med. 10, 739–743.

Muyzer, G., de Waal, E.C., and Uitterlinden, A.G. (1993). Profiling of complex microbial populations by denaturing gradient gel electrophoresis analysis of polymerase chain reaction-amplified genes coding for 16S rRNA. Appl. Environ. Microbiol. 59, 695–700.

Ohno-Urabe, S., Aoki, H., Nishihara, M., Furusho, A., Hirakata, S., Nishida, N., Ito, S., Hayashi, M., Yasukawa, H., Imaizumi, T., et al. (2018). Role of macrophage Socs3 in the pathogenesis of aortic dissection. J. Am. Heart Assoc. 7, e007389.

Oishi, Y., Spann, N.J., Link, V.M., Muse, E.D., Strid, T., Edillor, C., Kolar, M.J., Matsuzaka, T., Hayakawa, S., Tao, J., et al. (2017). SREBP1 contributes to resolution of pro-inflammatory TLR4 signaling by reprogramming fatty acid metabolism. Cell Metab. 25, 412–427.

Paradis, E., and Schliep, K. (2019). Ape 5.0: an environment for modern phylogenetics and evolutionary analyses in R. Bioinformatics 35, 526–528.

Qin, H., Wang, L., Feng, T., Elson, C.O., Niyongere, S.A., Lee, S.J., Reynolds, S.L., Weaver, C.T., Roarty, K., Serra, R., et al. (2009). TGF-beta promotes Th17 cell development through inhibition of SOCS3. J. Immunol. 183, 97–105.

Roberts, A.W., Robb, L., Rakar, S., Hartley, L., Cluse, L., Nicola, N.A., Metcalf, D., Hilton, D.J., and Alexander, W.S. (2001). Placental defects and embryonic lethality in mice lacking suppressor of cytokine signaling 3. Proc. Natl. Acad. Sci. U S A 98, 9324–9329.

Sachithanandan, N., Fam, B.C., Fynch, S., Dzamko, N., Watt, M.J., Wormald, S., Honeyman, J., Galic, S., Proietto, J., Andrikopoulos, S., et al. (2010). Liver-specific suppressor of cytokine signaling-3 deletion in mice enhances hepatic insulin sensitivity and lipogenesis resulting in fatty liver and obesity. Hepatology 52, 1632–1642.

Satake, S., Hirai, H., Hayashi, Y., Shime, N., Tamura, A., Yao, H., Yoshioka, S., Miura, Y., Inaba, T., Fujita, N., et al. (2012). C/EBPbeta is involved in the amplification of early granulocyte precursors during candidemia-induced "emergency" granulopoiesis. J. Immunol. 189, 4546–4555.

Seibler, J., Zevnik, B., Kuter-Luks, B., Andreas, S., Kern, H., Hennek, T., Rode, A., Heimann, C., Faust, N., Kauselmann, G., et al. (2003). Rapid generation of inducible mouse mutants. Nucleic Acids Res. 31, e12.

Swiderski, K., Thakur, S.S., Naim, T., Trieu, J., Chee, A., Stapleton, D.I., Koopman, R., and Lynch, G.S. (2016). Muscle-specific deletion of SOCS3 increases the early inflammatory response but does not affect regeneration after myotoxic injury. Skelet. Muscle 6, 36.

Tadokoro, Y., Hoshii, T., Yamazaki, S., Eto, K., Ema, H., Kobayashi, M., Ueno, M., Ohta, K., Arai, Y., Hara, E., et al. (2018). Spred1 safeguards hematopoietic homeostasis against diet-induced systemic stress. Cell Stem Cell 22, 713–725.e718.

Takahashi, S., Tomita, J., Nishioka, K., Hisada, T., and Nishijima, M. (2014). Development of a prokaryotic universal primer for simultaneous analysis of Bacteria and Archaea using next-generation sequencing. PLoS One 9, e105592.

Turnbaugh, P.J., Ley, R.E., Mahowald, M.A., Magrini, V., Mardis, E.R., and Gordon, J.I. (2006). An obesity-associated gut microbiome with increased capacity for energy harvest. Nature 444, 1027–1031.

Ueki, K., Kondo, T., Tseng, Y.H., and Kahn, C.R. (2004). Central role of suppressors of cytokine signaling proteins in hepatic steatosis, insulin resistance, and the metabolic syndrome in the mouse. Proc. Natl. Acad. Sci. U S A 101, 10422–10427.

Ushiki, T., Huntington, N.D., Glaser, S.P., Kiu, H., Georgiou, A., Zhang, J.G., Metcalf, D., Nicola, N.A., Roberts, A.W., and Alexander, W.S. (2016). Rapid inflammation in mice lacking both SOCS1 and SOCS3 in hematopoietic cells. PLoS One 11, e0162111.

STAR★METHODS

KEY RESOURCES TABLE

REAGENT or RESOURCE	SOURCE	IDENTIFIER
Antibodies		
PE anti-mouse CD3 (17A2)	BioLegend	Cat#100205
PE anti-mouse CD4 (GK1.5)	BioLegend	Cat#100408
PE anti-mouse CD8a (53-6.7)	BioLegend	Cat#100708
PE anti-mouse CD45R/B220 (RA3-6B2)	BioLegend	Cat#103207
PE anti-mouse CD19 (6D5)	BioLegend	Cat#115507
FITC anti-mouse/human CD11b(M1/70)	BioLegend	Cat#101205
APC anti-mouse Ly6G/Ly6C (Gr-1) (RB6-8C5)	BioLegend	Cat#108412
PE anti-mouse F4/80 antibody (BM8)	BioLegend	Cat#123110
PE anti-mouse TER-199/Erythroid cells (TER-119)	BioLegend	Cat#116207
PE/Cy7 anti-mouse CD117 (c-kit) (ACK2)	BioLegend	Cat#135111
APC anti-mouse Ly-6G antibody (1A8)	BioLegend	Cat#127613
FITC anti mouse CD34 (RAM34)	Thermo Fisher Scientific	Cat#11-0341-85
PE anti mouse CD117 (c-kit) (2B8)	BioLegend	Cat#105808
APC mouse lineage antibody cocktail	BD Biosciences	Cat#51-9003632
PE/Cy7 anti-mouse Ly-6A/E (Sca-1) (D7)	BioLegend	Cat#108114
APC/Cy7 anti mouse CD16/32 (93	BioLegend	Cat#101327
7-AAD	BD Biosciences	Cat#559925
Chemicals, peptides, and recombinant proteins		
Peanut oil	Sigma-Aldrich	Cat#P2144
Tamoxifen	Sigma-Aldrich	Cat#T5648
Metronidazole	Sigma-Aldrich	Cat#M3761
Vancomycin	Nacalai Tesque	Cat#36137-91
Ampicillin	Sigma-Aldrich	Cat#A9393
Neomycin	Sigma-Aldrich	Cat#N6386
High Fat Diet	Research diet, Inc.	D12492
Control Chow	Research diet, Inc.	D12450J
Critical commercial assays		
Cholesterol E-test	Fujifilm Wako Pure Chemical	Cat#439-17501
Triglyceride E-test	Fujifilm Wako Pure Chemical	Cat#432-40201
Luminex Assay Mouse Premixed Multi-Analyte Kit	R&D Systems	Cat#LXSAMSM-20
MethoCult	Stem Cell Technologies	Cat#M3534
Experimental models: Organisms/strains		
Socs3 floxed mice / C57BL/6	Kiu et al. (2007)	N/A
Rosa26-CreERT2 mice / C57BL/6	Seibler et al. (2003)	N/A
Vav-Cre mice / C57BL/6	Jackson Lab	Stock No: 008610
LysM-Cre mice / C57BL/6	RIKEN BRC	Stock No: RBRC02302
Oligonucleotides		
Primers for TaqMan Assay	Thermo Fisher Scientific	See Table S3
TaqMan Fast Advanced Master Mix	Thermo Fisher Scientific	Cat#4444557
SuperScript 3 Reverse Transcriptase	Thermo Fisher Scientific	Cat#18080093
RNaseOUT Recombinant Ribonuclease Inhibitor	Thermo Fisher Scientific	Cat#10777019

Continued		
REAGENT or RESOURCE	SOURCE	IDENTIFIER
dNTP Mix	Thermo Fisher Scientific	Cat#18427013
Oligo(dT)	Thermo Fisher Scientific	Cat#18418020
Software and algorithms		
FlowJo v.10.7.2.	FlowJo, LLC	https://www.flowjo.com
CytExpert ver 2.0	Beckman Coulter	https://www.beckman.com
GraphPad Prism v.6	Prism-graphpad.com	https://www.graphpad.com/scientific-software/prism/
RDP MultiClassifier ver.2.11	Michigan State University	http://rdp.cme.msu.edu/

RESOURCE AVAILABILITY

Lead contact

Further information and requests for resources and reagents should be directed to and will be fulfilled by the lead contact, Takashi Ushiki (tushiki@med.niigata-u.ac.jp).

Materials availability

This study did not generate new unique reagents.

Data and code availability

- 16S rRNA amplicon sequencing was performed at Techno Suruga Laboratory, Inc. (Shizuoka, Japan). Bacterial identification from sequences was performed using the TechnoSuruga Lab Microbial Identification database DB-BA 13.0 (TechnoSuruga Laboratory).

- Microbiome sequencing data have been deposited at the DDBJ Sequence Read Archive (http://trace.ddbj.nig.ac.jp/dra/) under accession number DRA012691.

- All original code is available in this paper's supplemental information.

- Any additional information requires to reanalyze the data reported in this paper is available from the lead contact upon request.

EXPERIMENTAL MODEL AND SUBJECT DETAILS

Animals and ethics statement

SOCS3 floxed (*Socs3^{fl}*), Rosa26-CreERT2, LysM-Cre, and Vav-Cre mice have been described previously (Clausen et al., 1999; Joseph et al., 2013; Kiu et al., 2007; Seibler et al., 2003); they were maintained in a C57BL/6 background. In experimental mice, the Rosa26-CreERT2 and Vav-Cre alleles were heterozygous and LysM-Cre was homozygous. 4 weeks old male and female mice were randomly assigned to experiments for 8-24 weeks. All animal experiments in this study were performed with the approval of the Animal Ethics Committees of Niigata University (SA00520, SD01054) or Walter and Eliza Hall Institute of Medical Research Animal Ethics Committee (2011.031, 2014.029).

METHOD DETAILS

Tamoxifen treatment and genotyping

Tamoxifen (4.2 mg for two doses after 4 days) was administered by oral gavage at 8 weeks of age, as previously described (Anastassiadis et al., 2010). PCR genotyping was performed using the following primers to distinguish the *Socs3^{+}* (613bp), *Socs3^{fl}* (740bp), and *Socs3^{-}* (288bp) alleles: 5′-ACGTCTGT GATGCTTTGCTG-3′, 5′-TCTTGTGTCTCTCCCCATCC-3′, and 5′-TGACGCTCAACGTGAAGAAG-3′.

High fat diet

Mice of all genotypes were fed an HFD (D12492; 60 kcal % fat, Research Diet Inc., New Brunswick, NJ, USA) or control chow (D12450J; 10 kcal % fat, Research diet, Inc.) from 4 weeks of age to the end of the observation period.

Antibiotics treatment

For intestinal tract microbiota depletion, mice were administered the following cocktail of four antibiotics (4Abx) in their drinking water from 4 weeks of age: ampicillin (Sigma-Aldrich, Merck KGaA, Darmstadt, Germany) 1 g/L, neomycin (Sigma-Aldrich) 1 g/L, metronidazole (Sigma-Aldrich) 1 g/L, and vancomycin (Nacalai Tesque, Inc., Kyoto, Japan) 500 mg/L. The 4Abx treatment was continued during the observation period.

Blood glucose measurement

Serum blood glucose was measured using blood collected from the retro-orbital plexus into Microtainer® tubes (BD Biosciences, Bedford, MA, USA) using Bio Majesty 6500 (JEOL Ltd., Tokyo, Japan). For the insulin tolerance test, 10-week-old mice were administered intraperitoneal insulin injections (0.375 U/kg body weight) following 5.5 h of fasting, blood was collected from the tail, and the glucose level was measured using a blood glucose meter.

Hepatic lipid analysis

Total lipids were extracted from the liver as previously described (Kuba et al., 2015). Hepatic T-Chol and TG were measured using the Cholesterol E-test and Triglyceride E-test (Fujifilm Wako Pure Chemical, Osaka, Japan).

Hematology and flow cytometry

Cells in blood collected from the retro-orbital plexus into Microtainer® tubes containing EDTA (BD biosciences, Bedford, MA, USA) were counted using Sysmex pocH-100iVDiff (Sysmex corporation, Kobe, Japan). Flow cytometric analysis was performed using CytoFLEX (Beckman coulter, NJ, USA). Antibodies were sourced from Biolegend (CA, USA): CD3 (17A2), CD4 (GK1.5), CD8 (53–6.7), Gr-1 (RB6-8C5), CD11b (M1/70), CD34 (RAM34), c-Kit (ACK2), Ly6G (1A8), CD19 (6D5), B220 (RA3-6B2), and TER119 (TER-119). LSK, CMP, GMP and megakaryocyte-erythroid progenitor (MEP) cells were counted as previously described (Katagiri et al., 2021). Granulocyte maturation was assessed based on the expression of c-kit and Ly6G as previously described (Figure S6) (Satake et al., 2012).

Colony assay

BM cells (2.0×10^4) were harvested from 8–10-week old mice and cultured in MethoCult M3534 (Stem Cell Technologies, Vancouver, Canada) according to the manufacturer's instructions. Total number of colonies, colony forming unit-granulocyte/macrophage (CFU-GM, CFU-G, and CFU-M), was scored after 7 days of culture.

RT-PCR analysis

The total RNA was isolated from the liver and colon using the RNeasy Mini kit (Qiagen, Hilden, Germany) according to the manufacturer's instructions. Regarding liver samples, RNA was collected without systemic perfusion. Reverse transcription of RNA to cDNA was performed using the SuperScript Reverse Transcriptase III kit (Thermo Fisher Scientific, MA, USA) with random hexamer primers. Each cDNA sample was analyzed using quantitative PCR with the StepOnePlus™ Real-Time PCR System (Thermo Fisher Scientific). Gene mRNA levels were determined by RT-qPCR using TaqMan probes (Thermo Fisher Scientific) (Table S3). Samples were run in triplicate and relative fold-changes in mRNA levels were calculated using the $2^{-\Delta\Delta Ct}$ method.

Cytokine Luminex assay

The serum concentrations of 20 cytokines (GM-CSF, CXCL1, TNFα, CCL2, IL-1β, S100A8, S100A9, IL-6, IL-10, IL-13, IL-17A, IFNγ, IL-3, Leptin, CCL5, G-CSF, IL-33, M-CSF, CCL3, and CCL4) were determined using the Luminex100/200 System (Luminex Corporation, TX, USA). Data were analyzed using MILLIPLEX Analyst 5.1 (EMD Millipore Corporation, MA, USA).

Physiological analyses

Mice were individually housed to monitor body weight and food intake. Oxygen consumption was measured at 30 days after tamoxifen administration using an O_2/CO_2 metabolic measurement system (Columbus Instruments, OH, USA), according to the manufacturer's instruction. Spontaneous activity levels were measured at 30 days after tamoxifen administration using the running wheel system and an open field

test. Using the Igloo Fast-Tracs Running Wheel system MK-713 (Muromachi Kikai, Tokyo, Japan), mice were housed individually in a cage containing this system, and the data were collected over 24 h using CompACT AMS Data Collection Software version 3.84 (Muromachi Kikai) following the training period for 12–16 h. In the open field test, each mouse was placed in the corner of an enclosed platform (40 cm × 40 cm × 30 cm), and the total distance traveled, time traveled, and time spent in the central area (20 cm × 20 cm) was recorded for 10 min.

Bacterial 16S rRNA amplicon sequencing and analysis

Fecal samples of mice at 30 days post-tamoxifen treatment were collected. 16S rRNA amplicon sequencing was performed at Techno Suruga Laboratory, Inc. (Shizuoka, Japan). In brief, bacterial genomic DNA was isolated as previously described (Takahashi et al., 2014). The V3-V4 hypervariable regions of the 16S rRNA were amplified from microbial genomic DNA using PCR with the bacterial universal primers (341F/R806) (Caporaso et al., 2011; Muyzer et al., 1993) and the dual-index method. All amplicons were sequenced on a MiSeq (Illumina, USA). The obtained read sequences on both sides were joined using fastq_join. After extracting a sequence with a QV of more than 20 with 99% or more bases in the sequence, the chimeric sequence was removed using USEARCH. Bacterial identification from sequences was performed using the TechnoSuruga Lab Microbial Identification database DB-BA 13.0 (TechnoSuruga Laboratory) and the results of RDP MultiClassifier ver.2.11 using Metagenome@KIN analysis software (World Fusion, Japan). Comparative analyses were also performed using Metagenome@KIN analysis software. In addition, we performed principal coordinate analysis (PCoA). The Euclidean distance was calculated using genus relative abundance in each sample. The PCoA was performed using the pcoa function in the R "ape" library (Paradis and Schliep, 2019).

QUANTIFICATION AND STATISTICAL ANALYSIS

Unless otherwise stated, data were analyzed using the analysis of variance (ANOVA) corrected for multiple testing. p values for specific comparisons were determined using GraphPad Prism (GraphPad Software, CA, USA). Further analyses are indicated in the figure legends. $P < 0.05$ was considered significant.